

PHOTOCOPY RESOLUTION TEST CHART

(4)

COLLEGE OF EARTH AND MINERAL SCIENCES

DEPARTMENT OF MATERIALS SCIENCE
METALLURGY PROGRAM

AD-A177 889

TECHNICAL REPORT

February 1987

OFFICE OF NAVAL RESEARCH

Contract No. N00014-84-k-0201

1. TYPES AND MODELS OF PRECIPITATION INDUCED NONUNIFORM GRAIN BOUNDARY CORROSION
2. INVESTIGATION OF SENSITIZATION AND GRAIN BOUNDARY CORROSION IN FERRITIC STAINLESS STEEL
3. THE LOCAL ELECTRODE POTENTIAL IN CAVITIES, CREVICES AND CRACKS AND ITS ROLE IN CAUSING DEGRADATION OF STRUCTURAL MATERIALS

R. N. Iyer, A. Valdes and H. W. Pickering

Department of Materials Science and Engineering
The Pennsylvania State University

DTIC
ELECTE
MAR 10 1987
S
A

THE PENNSYLVANIA STATE UNIVERSITY

College of Earth and Mineral Sciences

UNDERGRADUATE PROGRAMS OF STUDY

Ceramic Science and Engineering, Earth Sciences, Fuel Science, Geography, Geosciences, Metallurgy, Meteorology, Mineral Economics, Mining Engineering, Petroleum and Natural Gas Engineering, and Polymer Science.

GRADUATE PROGRAMS AND FIELDS OF RESEARCH

Ceramic Science, Fuel Science, Geochemistry and Mineralogy, Geography, Geology, Geophysics, Metallurgy, Meteorology, Mineral Economics, Mineral Processing, Mining Engineering, Petroleum and Natural Gas Engineering, and Polymer Science.

UNIVERSITY-WIDE INTERDISCIPLINARY GRADUATE PROGRAMS INVOLVING E&MS FACULTY AND STUDENTS

Earth Sciences, Ecology, Environmental Pollution Control Engineering, Mineral Engineering Management, Operations Research, Regional Planning, and Solid State Science.

ASSOCIATE DEGREE PROGRAMS

Metallurgical Engineering Technology and Mining Technology.

INTERDISCIPLINARY RESEARCH GROUPS WITHIN THE COLLEGE

Coal Research, Ore Deposits Research, Earth System Science, and the Mining and Mineral Resources Research Institute.

ANALYTICAL AND STRUCTURAL STUDIES

Classical chemical analysis of metals and silicate and carbonate rocks; X-ray crystallography; electron microscopy and diffraction; electron microprobe analysis; atomic absorption analysis; spectrochemical analysis; surface analysis by secondary ion mass spectrometry (SIMS); and scanning electron microscopy (SEM).

REPORT DOCUMENTATION PAGE		READ INSTRUCTIONS BEFORE COMPLETING FORM
1. REPORT NUMBER Technical Report, February 1987	2. GOVT ACCESSION NO. AD-A177889	3. RECIPIENT'S CATALOG NUMBER
4. TITLE (and Subtitle) Nonuniform Grain Boundary Corrosion and the Local Electrode Potential in Crevice	5. TYPE OF REPORT & PERIOD COVERED Technical Report	
	6. PERFORMING ORG. REPORT NUMBER	
7. AUTHOR(s) R. N. Iyer, A. Valdes, H. W. Pickering	8. CONTRACT OR GRANT NUMBER(s) N00014-84-k-0201	
9. PERFORMING ORGANIZATION NAME AND ADDRESS Metallurgy Program, 209 Steidle Building The Pennsylvania State University University Park, PA 16802	10. PROGRAM ELEMENT, PROJECT, TASK AREA & WORK UNIT NUMBERS	
11. CONTROLLING OFFICE NAME AND ADDRESS	12. REPORT DATE February 1987	
	13. NUMBER OF PAGES	
14. MONITORING AGENCY NAME & ADDRESS (if different from Controlling Office)	15. SECURITY CLASS. (of this report)	
	15a. DECLASSIFICATION/DOWNGRADING SCHEDULE	
16. DISTRIBUTION STATEMENT (of this Report)		
17. DISTRIBUTION STATEMENT (of the abstract entered in Block 20, if different from Report)		
18. SUPPLEMENTARY NOTES		
19. KEY WORDS (Continue on reverse side if necessary and identify by block number)		
20. ABSTRACT (Continue on reverse side if necessary and identify by block number) This Technical Report consists of three papers to be presented at the upcoming Conference on Environmental Degradation of Engineering Materials III to be held April 13-15, 1987 at The Pennsylvania State University, University Park, PA. The first two papers are on precipitation induced grain boundary corrosion, with a particular emphasis on sensitization in stainless steel. The third paper is on the importance of the local electrical potential on crevice and pit growth. <i>Keywords: Grain boundary corrosion, Crevice corrosion, Metal</i>		

DD FORM 1473

1 JAN 73

EDITION OF 1 NOV 65 IS OBSOLETE
S/N 0102-LF-014-6601

SECURITY CLASSIFICATION OF THIS PAGE (When Data Entered)

TYPES AND MODELS OF PRECIPITATION INDUCED NONUNIFORM
GRAIN BOUNDARY CORROSION

H. W. Pickering and R. N. Iyer
Department of Materials Science & Engineering
The Pennsylvania State University
University Park, PA 16802

Author	H. W. Pickering and R. N. Iyer
Title	TYPES AND MODELS OF PRECIPITATION INDUCED NONUNIFORM GRAIN BOUNDARY CORROSION
Source	
Availability Codes	
Special	

Presentation at: Conference on Environmental Degradation of Engineering Materials III, The Pennsylvania State University, April 1987.



ABSTRACT

This paper reviews recent progress on understanding precipitation induced grain boundary corrosion, with a particular emphasis on explaining the variable amounts of corrosion that can occur on different grain boundaries, or even along a single grain boundary, of a sample.

INTRODUCTION

Many examples of uneven grain boundary attack on a sample are available in the literature. Often, a comparison of different grain boundaries in a sample shows that they are not all attacked with the same severity. Some boundaries may be virtually unattacked while others exhibit wide trenches caused by the corrosive action. Consideration of the relative energies of the boundaries can usually account for the different degrees of precipitation and thereby for different responses to the corrosive solution; this is at least suggested in some recent results of sensitization in stainless steels [1].

There are, however, different ways in which unevenness of the corrosion can manifest itself and, thus, there may be more than one, and perhaps several, causes of uneven grain boundary attack. In considering a single grain boundary segment, the amount of attack on either side of the boundary can differ. A recent model [2,3] based on the two adjacent grains being of different size, can be used to explain this behavior for certain aging conditions [3]. Grain boundary motion could also be a factor, in particular, grain boundary motion that is induced by the diffusion or precipitation processes.

One can occasionally see a series of trenches along the length of a grain boundary separated by unattacked boundary segments. A recent finite difference model of the kinetics of sensitization in stainless steels shows

how the Cr concentration can vary along the length of a grain boundary [4,5]. The calculated Cr profiles from this model are consistent with the observation that grain boundaries can be sensitized over their entire length or only along segments of their length depending on the aging conditions.

Thus, there are different categories of uneven sensitization at grain boundaries. Those described above are illustrated in Figure 1. Although the situations in Figure 1 can be found in various alloy systems, most of the understanding of these features have come from investigations of, and the application of models to, ferritic and austenitic stainless steels.

In stainless steels, corrosive attack of the grain boundaries occurs after elevated temperature heat treatments that enable carbides to form at the grain boundaries. The steel is referred to as sensitized if certain corrosives attack these boundaries. The corrosive attack of sensitized stainless steel is generally accepted to be explained by the chromium-depletion theory [6,7], although the completeness of this theory is now open to question [1]. In this theory chromium rich carbides form in the grain boundaries, thereby depleting the adjacent alloy of chromium, and it is this chromium depleted material that is susceptible to corrosive attack. The need for a more complete theory follows from the observation that the width of the attacked region at sensitized grain boundaries is usually several times larger than the width of the Cr-depleted zone produced by the carbide precipitation process [1].

Over the years an explanation of why the Cr-depleted material is more susceptible to corrosion has developed around the well known relationship of an increased tendency for passivation with increasing Cr content of the stainless steel. This is nicely illustrated in the experimental results of Frankenthal and Pickering [8]. Thus, the open circuit potentials of corrosives used to test for sensitization, e.g., the Strauss test, are in the range of the active/passive transition for chromium contents below approximately 13%. A consequence of the theory is that the corrosive action is confined to the Cr-depleted alloy, i.e., the corrosive attack would not propagate into the adjacent alloy of bulk Cr content. Since, in fact, bulk alloy adjoining the Cr-depleted material is corroded during grain boundary corrosion of sensitized stainless steels, some modification or extension of the Cr-depletion theory is needed. Just what that modification should be remains to be seen. One possibility is the initiation of a localized corrosion process following the formation of the crevice-like cavity during attack of the Cr-depleted material [1].

RESULTS

A brief review follows of the above mentioned modeling and experimental results that give some insight into some or all of the types of grain boundary corrosion mentioned above and depicted in Figure 1. Most of the

PRECIPITATION INDUCED NONUNIFORM GRAIN BOUNDARY CORROSION

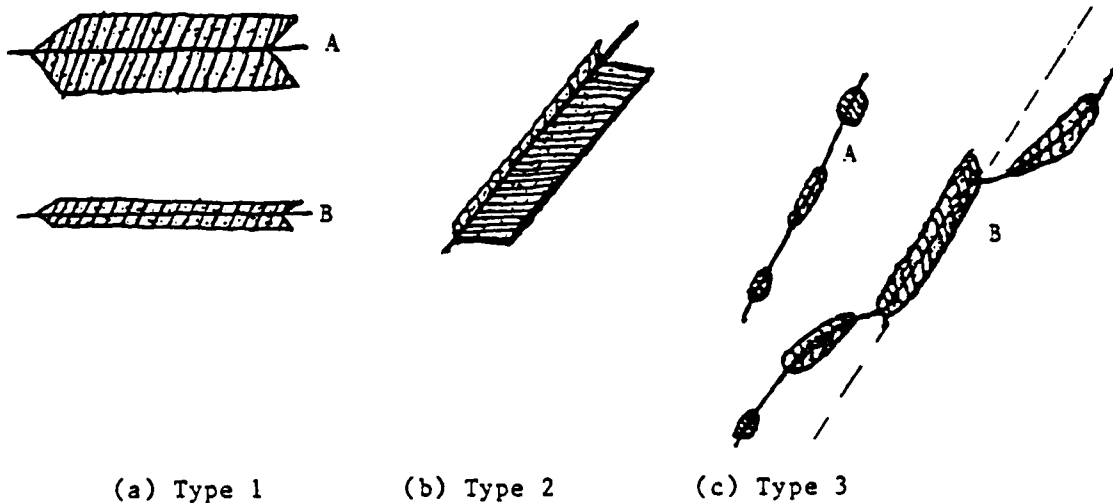


Figure 1. Schematic diagram showing three types of nonuniform grain boundary corrosion (a) from boundary A to boundary B (Type 1) (b) on either side of a boundary (Type 2) (c) along a single boundary (Type 3).

progress made on the subject is current and has only recently, or soon will, appear in the literature. The topic of uneven grain boundary attack is timely since it has not recently been a part of symposia on sensitization or grain boundary corrosion. When referring to uneven grain boundary attack in what follows, Types 1, 2 and 3 correspond to the three classifications in Figure 1a, b and c, respectively.

Type 1 Grain Boundary Corrosion

Because the structures of grain boundaries and the habit plane relationships between the grain boundary precipitates and the grains vary from boundary to boundary, e.g., from Boundary A to Boundary B in Figure 1a, the Type 1 behavior shown in Figure 1a is to be expected. There is, however, only qualitative understanding of the phenomena based on a scarcity of research to the present time. Work by Erb et.al. [9] on Cu, by Arora and Metzger [10] on Al and by others [11,12] was helpful in this regard. The recent emphasis of this problem is due to Bennett [4]. His studies of sensitization in austenitic and ferritic stainless steel were on the influence of misorientation angle, grain boundary structure and habit plane on the variation in kinetics of sensitization among the boundaries of a sample. To establish grain boundary atomic structure, orientation information of the adjacent grains, obtained with the electron backscattering (EBS) technique [13,14], was combined with the SEM image of the surface to obtain the orientation of the grain boundary. Modeling of

the grain boundary structure was based on ideal crystallography and the coincident site lattice concept. The results support the concepts (1) of a threshold misorientation angle whose value is a function of the aging time and temperature, below which boundaries are of sufficiently low energy that sensitization does not occur, and (2) of a major role of grain boundary structure in explaining the wide variation in sensitization that occurs in grain boundaries having misorientation angles greater than the threshold value. These concepts are reviewed in some detail in another paper in this session [15]. This explanation of Type 1 behavior considers the nucleation and growth of the grain boundary precipitates as unique functions of the boundary structure.

The role of the habit plane relationship between the precipitate and the grains forming the boundary could also be a factor in Type 1 attack. In particular, habit plane effects are expected to be more predominant in low angle ($< 15^\circ$) grain boundaries, and grain boundary structure effects be more significant in higher angle grain boundaries. This is due to the fact that low angle grain boundaries consist of the same $\{h k l\}$ planes tilted to each other with the space in between accommodated by a dislocation network. If the $\{h k l\}$ plane is a matching plane for carbide precipitation, the grain boundary will be a favored interface for precipitation. However, for a high angle grain boundary, the grain boundary energy is high enough to facilitate carbide precipitation without the need of a habit plane match. These aspects are discussed in detail in an upcoming paper [3]. Both grain boundary structure and habit plane effects are accentuated during nucleation and initial growth of the carbide precipitate. Therefore, consequence of these effects will be best seen in a quenched/air-cooled ferritic stainless steel for which $C > 0.03\%$ or in a shortly aged austenitic stainless steel. For longer aging times, the kinetics of carbide growth will be affected by grain size, especially in cases of limited carbon supply for the ferritic stainless steels.

Considering again metal carbide as the precipitate, in cases of limited carbon supply, another explanation of Type 1 behavior is based on grain size. The salient point is that the larger is the volume element supplying carbon to unit area of grain boundary, the more extensive will be the sensitization per unit area. Assuming spherical grains of radius r , since the area of the grain boundary per unit grain volume will be a decreasing function of r , grain boundaries formed by large grains (Type A in Figure 1a) will be more heavily sensitized than those formed by small grains (Type B in Figure 1a). Since the greater the sensitization, the wider is the width of the Cr-depleted layer, a corrosive solution produces Type 1 behavior; but in this case, there is a unique relationship between the width of the Cr-depleted layer and the size of the grains at each grain boundary. A limited carbon supply is more likely to become a factor for alloys with a low carbon content and/or small grain size. The grain size effect in sensitization is described elsewhere [2,3] and is summarized in another

PRECIPITATION INDUCED NONUNIFORM GRAIN BOUNDARY CORROSION

paper in this session [15].

Type 2 Grain Boundary Corrosion

When a greater attack occurs on one side of a grain boundary, as illustrated in Figure 1b, both habit plane and grain size could be factors. A favorable habit plane relationship, especially for a low angle grain boundary, between the precipitate and one of the two grains forming the boundary favors growth of the precipitate into that grain. The chromium sustaining growth of the precipitate also comes from the same grain and so its Cr-depleted layer is of greater width than that on the other side of the boundary.

Similarly, when a grain boundary is bounded by grains of different size and providing the mass transport conditions and carbon content of the alloy are in the appropriate ranges, the grain size effect can cause Type 2 behavior. For the reasons given under Type 1 behavior, the width of the corrosive attack is greater on the side bounded by the larger grain.

Type 3 Grain Boundary Corrosion

In some commercial, relatively large grained ferritic stainless steels the metal carbides nucleate and grow so fast that it is common to find a sheet-like distribution of carbide covering most or all of the grain boundary network following a quench from the annealing temperature. In this case the Cr level along the boundary may be nearly uniform. This is the situation for which many kinetic models of sensitization are applicable [2,3,16,17]. If the kinetics of the interface reaction and of carbon transport are fast relative to the transport of Cr, the uniform Cr concentration will be that coexisting with the carbide and the bulk carbon concentration. Otherwise, the uniform Cr concentration at the interface will lie somewhere between this value and the bulk Cr concentration.

On the other hand, in the austenitic stainless steels for which the Cr diffusivity is almost two orders of magnitude lower and the C diffusivity is almost three orders of magnitude lower, and in other ferritic stainless steels of lower carbon level or smaller grain size for which the supply of carbon becomes a factor, only relatively few carbides are usually found along the grain boundaries following the quench [14]; as a result, the Cr level can be quite inhomogeneous along the boundary. In this case the carbide spacing and the subsequent aging conditions become factors in the uniformity, or lack thereof, of sensitization along the length of a grain boundary. This situation could be a cause of Type 3 behavior, and is treated in a recent new general model of precipitation at grain boundaries developed by Bennett [4,5].

When considering variations in the precipitation kinetics at a single

grain boundary, other factors that normally have primary importance can be much less important, i.e., habit plane relationship and grain size. However, grain boundary structure could be a factor in that there might be regions of high coincidence and other regions of large misfit. Regions of large misfit would be accommodated by various defects that could act as excellent sites for carbide nucleation and growth. Due to such inhomogeneity along a boundary, the kinetics of growth differ. Thus, diffusion fields would develop both perpendicular and parallel to such a boundary.

A major advantage of the Bennett model is that it considers overlapping diffusion fields within the grain boundary. Numerical (finite difference) calculations were used to accomplish this in the modeling. This sharply contrasts with analytical solutions (error function or series type) that have practical range limitations (i.e., short or long times). The model accounts for rapid diffusion within a grain boundary (x direction) between two lath-like precipitates. The slower volume diffusion is assumed to occur only normal to the boundary (y direction). In this manner, concentration profiles develop both in and normal to the grain boundary. Most importantly for application of the model to sensitization in stainless steels, the critical regime when neighboring Cr diffusion fields first overlap within the boundary can be closely followed. The major assumptions of the model [5] are (1) the grain boundary precipitates have a lath-like morphology; therefore, diffusion fields in the boundary are planar. (2) Diffusion only occurs in the x direction within the grain boundary and in the y direction within the bulk of the grain. (3) The precipitate-matrix interface remains relatively stationary during the grain boundary precipitation process (as compared to the average distance between precipitates). (4) Diffusion of one component of the precipitate (Cr in the case of stainless steel) is much slower than that of other components (carbon) so that its transport completely determines the precipitate growth rate. These assumptions are reasonable for application of the model to the stainless steels, in particular the austenitic stainless steels. In the case of the ferritic stainless steels assumption (3) comes into question because of the relatively small metal carbide spacing.

Since the model includes sensitization time and temperature, precipitate spacing, grain boundary and volume diffusivity, and grain boundary width as parameters, it provides a powerful means to theoretically investigate the sensitization process. Typical calculated profiles for an austenitic stainless steel containing 18% Cr are shown in Figure 2. The suitability of the model for the austenitic stainless steels is supported by the good agreement with the experimental results of Hall and Briant [18] who determined the chromium profiles in and normal to the grain boundary for a situation where the carbides were so widely spaced that the chromium diffusion fields within the boundary did not overlap even after 100 hours of aging at 700°C. To simulate these experimental conditions, the carbide spacing was set at 10 μm and the diffusion coefficients and interface

PRECIPITATION INDUCED NONUNIFORM GRAIN BOUNDARY CORROSION

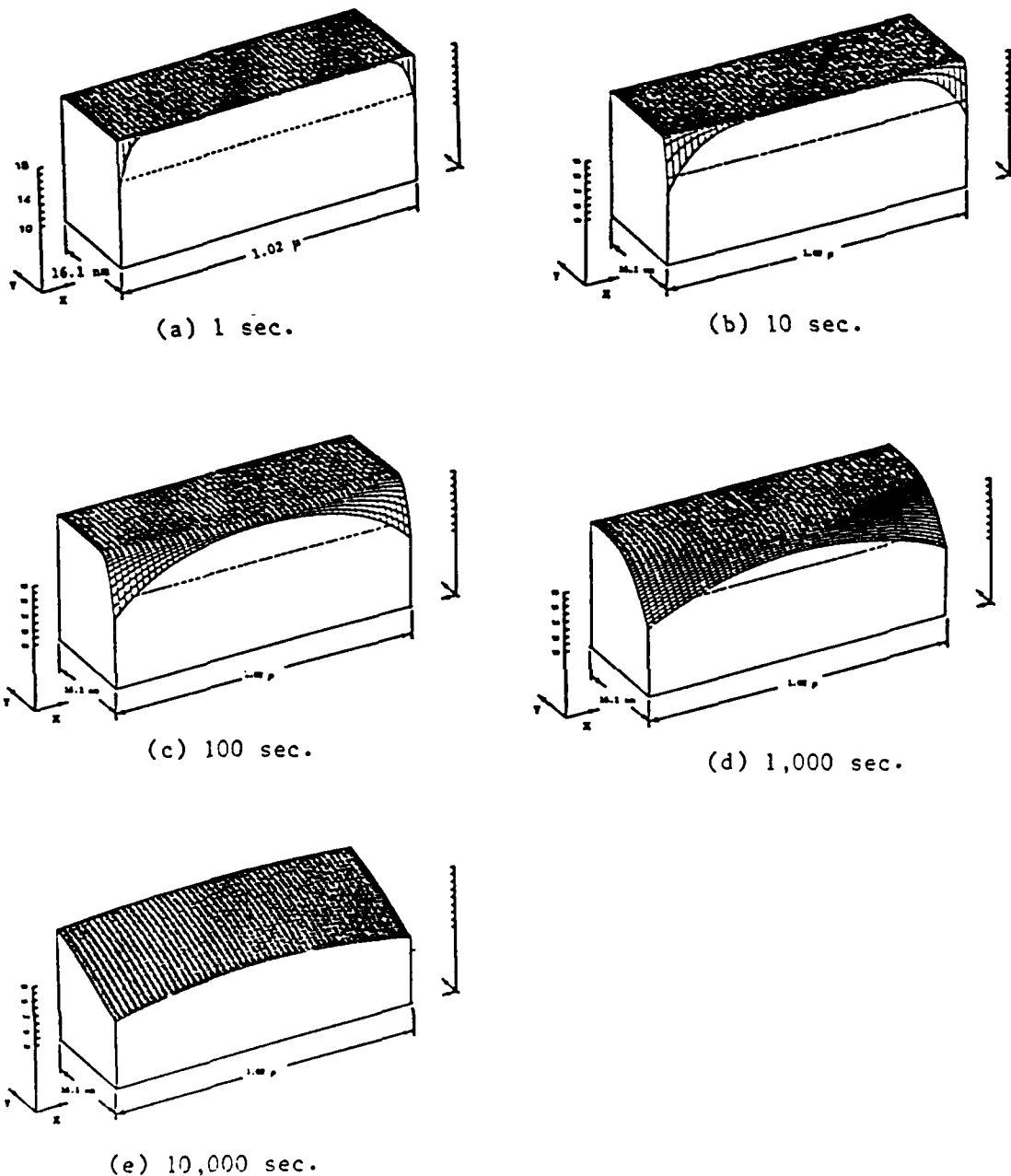


Figure 2. Calculated Cr concentration profiles in the boundary (x direction) and normal to the boundary into one of the adjacent grains (y) for a carbide spacing of $1.02 \mu\text{m}$ in a type 304 austenitic stainless steel aged at 650°C for various times. Cr concentration is plotted along the vertical axis (z direction). [4].

compositions for 700°C were used. Calculated results using the model [4,5] and the experimental data of Hall and Briant [18] are shown in Figures 3a and 3b. Both the calculated and experimental profiles normal to the boundary in Figure 3b are for a grain boundary position approximately 0.2 μm away from the carbide (in the x direction within the grain boundary plane).

Defining a fully sensitized boundary as one in which the Cr level is below 13 at. % everywhere along the boundary, the calculated time for sensitization was found to agree well with experimental times, e.g. the calculated time for the simulation shown in Figure 2 was 2160 seconds [5] of aging compared with experimental results which showed that most boundaries in a Type 304 stainless steel were fully sensitized between 1800 and 2700 seconds of isothermal aging at 650°C [1]. Therefore, this model has the property of being able to estimate sensitization times. This is true for both a bulk alloy, where the model parameters are average properties (i.e. carbide spacings and diffusivities) and a single grain boundary, where the parameters are unique properties of the boundary [1,4]. The accuracy of the calculated sensitization time depends primarily on how well the spacing of the carbides is known for a given aging temperature and alloy composition. Thus, since the model describes a process which is both nucleation and growth dependent, the role of nucleation of the precipitate still needs to be included in a complete model, in which case sensitization time could be calculated without a knowledge of the precipitate spacing.

Based on the above definition of a fully sensitized boundary, uneven attack of the type depicted in Figure 1c could occur for a partially sensitized condition where grain boundary segments, but not the entire length of the boundary, fall below the 13% Cr level. This explanation may be oversimplified for some observations of Type 3B behavior (Figure 1). In this case, diffusion induced grain boundary motion (DIGM) may be involved. But whether Cr diffusion can cause this phenomenon has not yet been investigated. Another possibility is that the growing carbide laths can induce grain boundary motion to minimize excessive interfacial energies: this may be termed precipitation induced grain boundary motion (PIGM).

CONCLUSIONS

1. Three types of nonuniform grain boundary corrosion are identified. These are the variants (a) from grain boundary to grain boundary of a sample (Type 1), (b) along either side of a boundary (Type 2), and (c) along a grain boundary (Type 3).
2. Each of the above three types of nonuniform grain boundary corrosion is discussed as to the possible causes, for the case of precipitation induced grain boundary corrosion.

PRECIPITATION INDUCED NONUNIFORM GRAIN BOUNDARY CORROSION

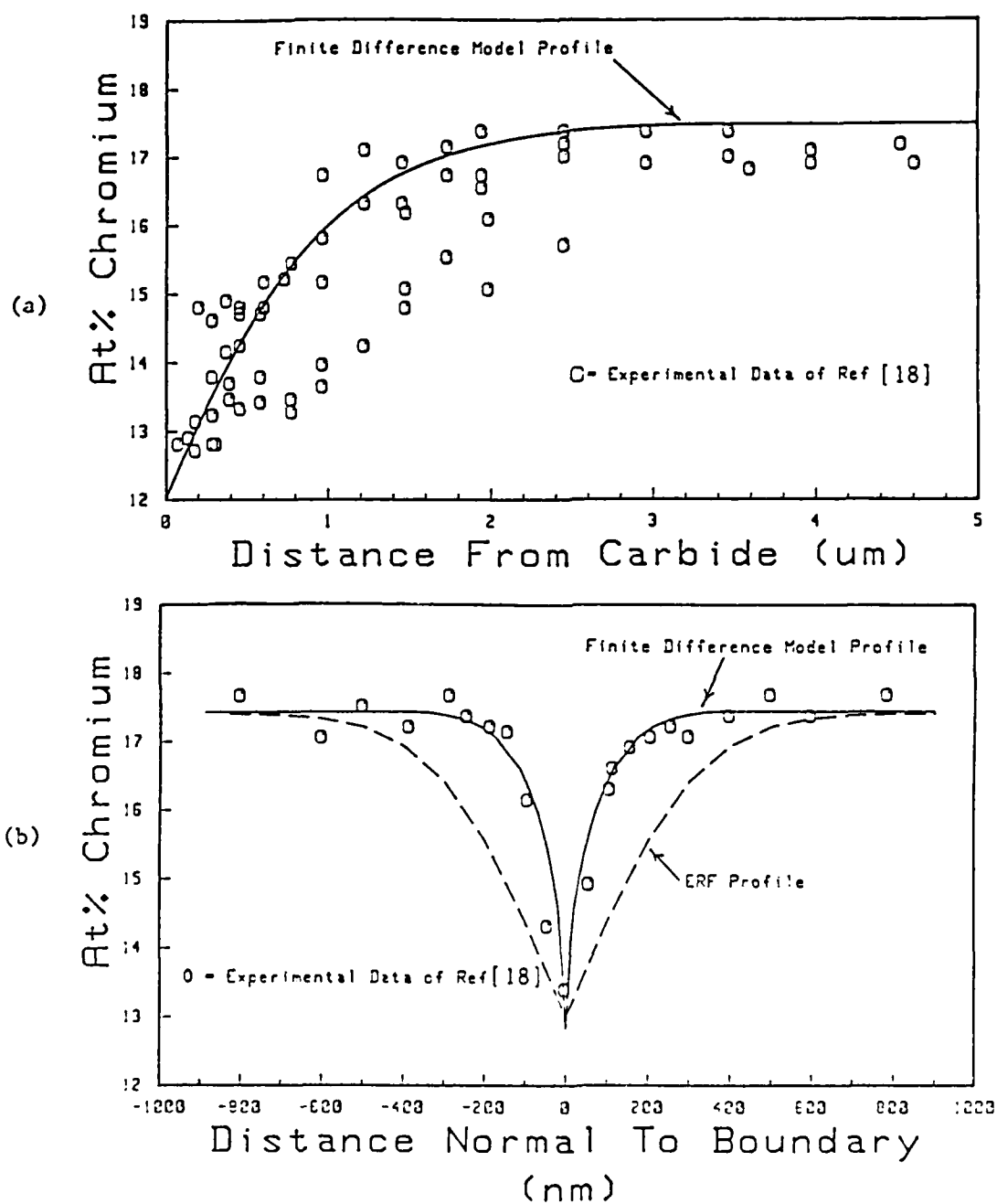


Figure 3. Calculated Cr concentration profiles. (a) in, and (b) normal to the grain boundary after aging 100 hrs. at 700°C for a carbide spacing of 10 μm in type 304 austenitic stainless steel. [4].

3. A review is given of the different factors known to contribute to nonuniform grain boundary corrosion. These include (a) grain boundary structure, (b) habit plane relationship with the precipitate, (c) misorientation angle, (4) grain size and (5) diffusion/precipitation induced grain boundary motion.

ACKNOWLEDGEMENT

The financial support of the Office of Naval Research under Contract No. N00014-84-K-0201 is gratefully acknowledged.

REFERENCES

1. B. W. Bennett and H. W. Pickering, Metall. Trans. A, 18A (June, 1987).
2. G. S. Was and R. M. Kruger, Acta Metall., 33, 841 (1985).
3. R. N. Iyer and H. W. Pickering, to be submitted to Metall. Trans. A.
4. B. W. Bennett, Ph.D. Thesis, The Pennsylvania State University, 1984.
5. B. W. Bennett and H. W. Pickering, Submitted to Acta Metall.
6. B. Strauss, H. Schottky and J. Hinnuber, Z. anorg. allgem. Chem, 188, 309 (1930).
7. E. C. Bain, R. H. Aborn and J.J. B. Rutherford, Trans. Am. Soc. Steel Treating, 21, 481 (1933).
8. R. P. Frankenthal and H. W. Pickering, J. Electrochem. Soc., 120, 23 (1973).
9. U. Erb, H. Gleiter and G. Schwitzgebel, Acta Metall., 30, 1377 (1982).
10. O. P. Arora and M. Metzger, Trans. Metall. LSoc. AIME, 236, 1205 (1966).
11. J. Y. Boos, C. Goux, Compt. Rend., C271, 978 (1971).
12. M. Froment and C. Vignaud, C272, 165 (1972).
13. J. A. Venables and C. J. Harland, Phil. Mag., Ser. A, 27, 1193 (1973).
14. B. W. Bennett and H. W. Pickering, Scripta Metall., 18, 743 (1984).
15. R. N. Iyer and H. W. Pickering, this proceedings, p. ?
16. C. Stawstrom and M. Hillert, J. Iron Steel Inst., 207, 77 (1969).
17. T. Thorvaldsson and A. Salwen, Scripta Met., 18, 739 (1984).
18. E. L. Hall and C. L. Briant, Metall. Trans. A, 15A, 793 (1984).

**INVESTIGATION OF SENSITIZATION AND GRAIN BOUNDARY
CORROSION IN FERRITIC STAINLESS STEEL**

**R. N. Iyer & H. W. Pickering
Department of Materials Science and Engineering
The Pennsylvania State University
University Park, PA 16802**

**Presentation at: Conference on Environmental Degradation
of Engineering Materials III, The Pennsylvania State
University, April 1987.**

ABSTRACT

Thermodynamic modeling of sensitization in ferritic stainless steel, using the Kohler formulation and interaction parameters from phase diagrams, yields the specific interfacial chromium concentration at the carbide-matrix interface as a function of the carbon and chromium concentrations and sensitization temperature. Using an electrochemical measuring technique, the level of chromium in the Cr-depleted material of a Fe-16.5Cr-0.055C steel aged at different temperatures was estimated. Temperature dependence of this measured chromium content correlates fairly well with that predicted by the model. Kinetic modeling and experimental results indicate that differences in sensitization and intergranular corrosion among grain boundaries in a sample are based on grain boundary structure, habit plane and/or grain size.

INTRODUCTION

The problem of sensitization in stainless steels and the consequent susceptibility to intergranular corrosion have been studied for a long time [1-5]. Most of the studies, especially the recent works, have concentrated on the austenitic stainless steels. The sensitization process that causes Cr depletion at grain boundaries has been modeled on the basis of limiting Cr diffusion to the grain boundaries where Fe-Cr carbides typically $(CrFe)_{23}C_6$ form [3,6,7]. Sensitization and intergranular corrosion are influenced by grain boundary structure, as has been shown in a recent study [8].

The development of Cr depleted zones in sensitized alloys depends on both thermodynamic and kinetic conditions for carbide precipitation and growth. There are minimum levels of Cr and C that are in quasi-equilibrium at the carbide-matrix interface [5,9,10]. This interfacial Cr concentration depends on temperature and alloy composition, particularly bulk C concentration, as shown by Was and Kruger [9] for Ni-Cr-Fe alloys.

In this paper, a model is developed for Fe-Cr alloys patterned after the Was and Kruger model. It incorporates the effects of temperature and alloy composition with particular reference to the carbon concentration for

calculating the minimum Cr concentration in the Cr-depleted zones next to the grain boundary carbides.

THERMODYNAMIC ANALYSIS

Combining the free energy change of carbide precipitation (ΔG) with the activities of the components, derived from solid solution interaction parameters, the carbide-matrix interfacial concentrations of Cr and C can be computed. The following analysis of the Fe-Cr-C system is similar to the approach utilized by Was and Kruger [9] for the Ni-Cr-Fe system.

The formation of Cr,Fe carbide can be described generally by the reaction



where the free energy change

$$\begin{aligned} (\Delta G)_{\text{Cr}_m\text{Fe}_n\text{C}} &= G_{\text{Cr}_m\text{Fe}_n\text{C}} - m G_{\text{Cr}} - n G_{\text{Fe}} - G_{\text{C}} = -RT \ln \left(\frac{a_{\text{Cr}_m\text{Fe}_n\text{C}}}{a_{\text{Cr}}^m a_{\text{Fe}}^n a_{\text{C}}} \right) \\ &= -RT \ln a_{\text{Cr}_m\text{Fe}_n\text{C}} + mRT \ln a_{\text{Cr}} + nRT \ln a_{\text{Fe}} + RT \ln a_{\text{C}} \quad (1) \end{aligned}$$

The free energy of the Fe-Cr-C solid solution (G^{bcc}) can be described in terms of the Kohler formulation [11] as:

$$G^{\text{bcc}} = \sum_i x_i G_i^{\text{bcc}} + RT \sum_i x_i \ln x_i + \sum_{ij} \frac{x_i x_j}{(x_i + x_j)} (x_i g_{ij} + x_j g_{ji}) \quad (2)$$

where G_i^{bcc} is the free energy of pure component i in the bcc phase, relative to its reference state (i.e., G_i^{bcc} represents the lattice stability values for the alloy components). x_i is the atom fraction of component i , i.e.,

$$\sum_i x_i = 1 \quad (3)$$

g_{ij} is the binary interaction parameter between a pair of components i and j . These quantities are obtained from calculations based on binary phase diagrams [12-14]. In general, $g_{ij} \neq g_{ji}$ and R and T have their usual meanings.

The partial molar free energy of the i^{th} component (\bar{G}_i) is given by:

SENSITIZATION AND GRAIN BOUNDARY CORROSION

$$\bar{G}_i = G_i^{bcc \rightarrow \text{ref. state}} + RT \ln x_i + \sum_j \left\{ \frac{x_i x_j}{(x_i + x_j)} \left[\frac{x_j}{(x_i + x_j)} + (1 - x_i) \right] g_{ij} \right\} + \sum_j \left\{ \frac{x_j^2}{(x_i + x_j)} \left[\frac{x_j}{(x_i + x_j)} - x_i \right] g_{ji} \right\} - \sum_{j1} \left\{ \frac{x_j^2 x}{(x_j + x_1)} g_{j1} \right\} + (\bar{G}_i)^{\text{ter}} \quad (4)$$

where i, j or 1 represent Cr, Fe or C; $j \neq i$; $1 \neq i, j$; and $(\bar{G}_i)^{\text{ter}}$ is the ternary term, signifying Fe-Cr-C interactions.

In terms of activities, a_i , of the components,

$$\bar{G}_i = RT \ln a_i \quad (5)$$

Equations (1), (3), (4) and (5) can be solved simultaneously in order to determine the interfacial Cr and C for a given alloy that forms carbide of known formula.

A specific case is solved here for Fe-16.5Cr alloy forming $(\text{FeCr})_{23} \text{C}_6$, which is the normal carbide type found in sensitized ferritic stainless steels [4,15]. The following assumptions are made:

- (1) The carbon activity remains spatially uniform. This assumption is validated by the fact that the diffusion coefficient of carbon is several orders of magnitude larger than that of chromium.
- (2) The carbide-matrix interface is at local equilibrium.

The carbide $(\text{CrFe})_{23} \text{C}_6$ can be written as $(\text{CrFe})_{23/6} \text{C}$ in which the individual chromium and iron contents, m and n in $\text{Cr}_m \text{Fe}_n \text{C}$ are taken from the literature [10,16], i.e., $n+m=23/6$. For 25% Cr steel, the carbide is of the form $\text{Cr}_{17} \text{Fe}_6 \text{C}_6$ [16] (or $\text{Cr}_{17/6} \text{Fe}_6 \text{C}$), and for 2.25% Cr steel it is

$\text{Cr}_9 \text{Fe}_{14} \text{C}_6$ [10] (or $\text{Cr}_{9/6} \text{Fe}_{14/6} \text{C}$). Utilizing these values, $m = (23/6) (x_{\text{Cr}})^{0.25}$ where x_{Cr} is the atom fraction of Cr in the alloy.

The free energy change $(\Delta G)_{\text{Cr}_m \text{Fe}_n \text{C}}$ can be obtained [12,13] as:

$(\Delta G)_{\text{Cr}_m \text{Fe}_n \text{C}} = A + BT + CT^2 + DT^3$, where A, B, C and D are constants that depend on the alloy composition.

For 16.5% Cr steel, $n = \frac{8}{6}$, $m = \frac{15}{6}$ and so

$$(\Delta G)_{Cr_{15/6}Fe_{8/6}C} = -3810 - 9.6T - 4.47 \times 10^{-3} T^2 + 3 \times 10^{-5} T^3 \text{ (cal/mole)}$$

The values of the binary interaction parameters (g_{ij}) and $G_i^{bcc \rightarrow \text{ref. state}}$ for the Fe-Cr system [17,19] are given in Table I.

Table I: Binary interaction parameters (g_{ij}) and Free Energies (G_i)

Components:	Cr-Fe(=Fe-Cr)	Cr-C(=C-Cr)	Fe-C	C-Fe
g_{ij} (cal/mole):	$6000 - 2.5T$	-32000	$-8400 - 9.04T$	$-22900 - 6.95T$
$G_{Cr}^{bcc \rightarrow bcc} = 0$; $G_{Fe}^{bcc \rightarrow bcc} = 0$; $G_C^{bcc \rightarrow \text{graphite}} = 35100 - 3.5T$ (cal/mole)				

The system of equations (1), (3), (4) and (5) are reduced to two nonlinear equations in x_{Cr} and x_C . These are then solved by a completely discretized Newton-Raphson procedure [17,18]. The ternary term, $(\bar{G}_i)^{ter}$ is obtained by using the formulation of Hillert [19] as follows:

$$\begin{aligned} (\bar{G}_{Cr})^{ter} &= x_{Fe} x_C (1-x_{Cr}) H_T \\ (\bar{G}_C)^{ter} &= x_{Cr} x_{Fe} (1-x_C) H_T \\ (\bar{G}_{Fe})^{ter} &= -x_{Cr} x_{Fe} x_C H_T \end{aligned} \quad (6)$$

so that, $(G)^{ter} = x_{Cr} \bar{G}_{Cr} + x_C \bar{G}_C + x_{Fe} \bar{G}_{Fe} = x_{Cr} x_{Fe} x_C H_T$.

H_T , the temperature dependent parameter, was found by iteration to satisfy the carbon solubility constraint at each temperature. Carbon solubility is obtained from the Fe-Cr-C phase diagram [20] as: $\ln(W_C) = 9.4 - 15000/T$, where $W_C = \text{wt\% C}$.

Analytically, H_T is given by

$$H_T = -49359 + 42.86T - 5.44 \times 10^{-2} T^2 + 2.69 \times 10^{-5} T^3 \text{ (cal/mole)} \quad (7)$$

The interfacial Cr concentration ($x_{Cr,i}$) is plotted against temperature, for different bulk carbon concentrations, in Figure 1. It can be seen that $(x_{Cr,i})$ increases with temperature, but decreases with increasing carbon concentration, which is consistent with literature findings.

EXPERIMENTAL

The electrochemical technique of potentiostatic polarization, used by Frankenthal and Pickering [4] has been utilized to assess the minimum level of chromium in the depleted zone of sensitized alloys. This technique is

SENSITIZATION AND GRAIN BOUNDARY CORROSION

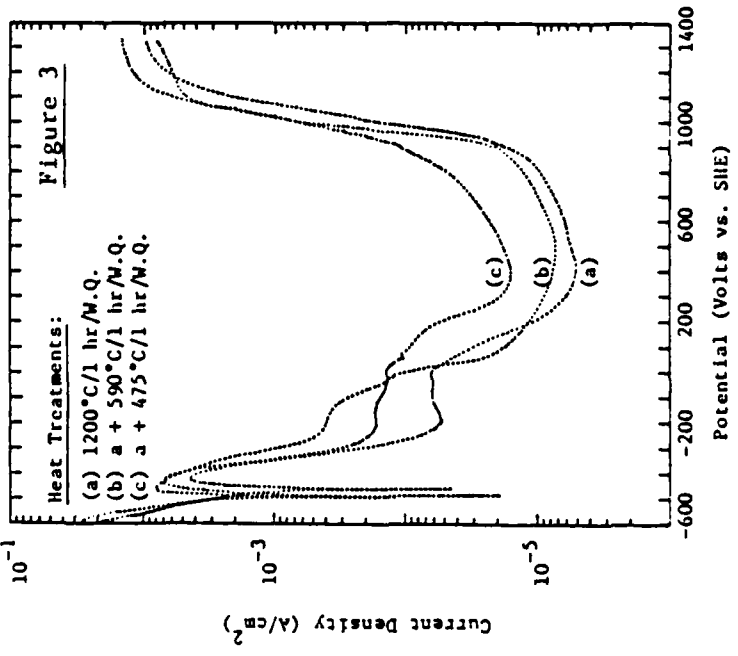
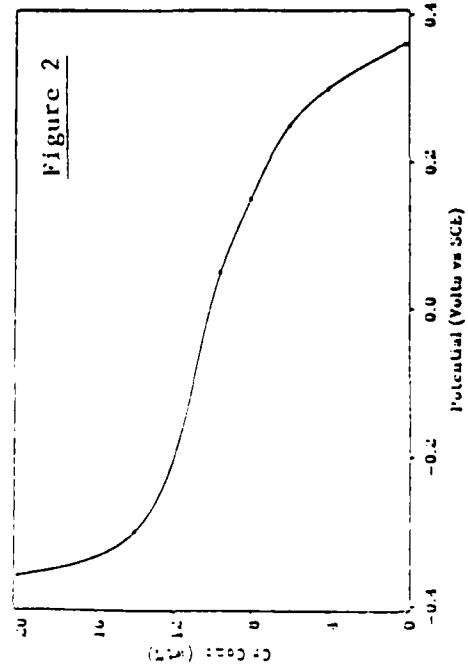
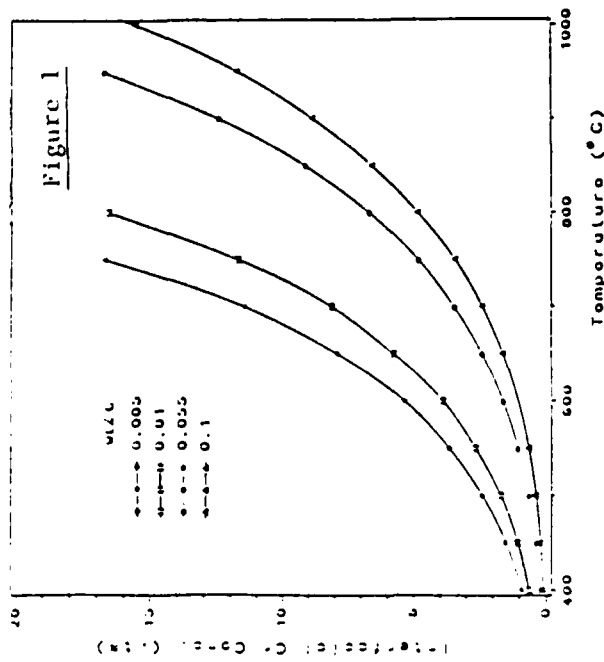


Figure 1. Calculated carbide-matrix interfacial chromium concentration vs. aging temperature for different bulk carbon concentrations in a Fe-16.5Cr alloy.

Figure 2. Cr concentration vs. passivation potential in Fe-Cr alloys [4].

Figure 3. Polarization curves for 430 S.S. in H₂SO₄ solution (deaerated with argon) at room temperature (scan rate = 0.1 mV/sec).

based upon the fact that the passivation potential of Fe-Cr solid solutions is a strong function of their Cr contents. The passivation potentials, experimentally determined for ferritic Fe-Cr alloys in 1N H₂SO₄ solution as a function of Cr concentration by Frankenthal and Pickering²[4], are plotted in Figure 2. Thus, the Strauss test, which has a potential of about 100 mV_{SCE} [21], will corrode depleted zones in ferritic stainless steel with Cr concentrations less than approximately 10% [4]. The critical Cr concentration below which a stainless steel loses its immunity to corrosion is about 13%.

The principal alloy investigated was a commercially available 430 stainless steel with the following chemical composition (wt%): Cr-16.46, Ni-0.32, Mo-0.024, Mn-0.48, Si-0.36, C-0.055, N-0.016, P-0.035, S-0.004. Coupons, 1cm x 3cm, were cut from cold rolled, annealed and pickled 0.12cm thick sheets of the steel and given the following heat treatments:

- A. 1 hr annealing at 1200°C, followed by a water quench
- B. As in A + 1 hr aging at 475°C or 590°C, followed by a water quench

All of the heat-treatments were carried out on specimens encapsulated in Vycor glass under vacuum, after intermittent purging by argon gas, to prevent oxidation and Cr loss during heating. Following the heat-treatments, specimens were polished, using finally 0.05 μm alumina powder.

Electrochemical tests were carried out in three-electrode cells, using platinum gauze as the counter electrode and a saturated calomel reference electrode. The electrolyte solution was 1N H₂SO₄, deaerated with argon at ambient temperature. The potentials were applied using a potentiostat interfaced to a personal computer, which recorded the potential, current and elapsed time.

Tested specimens were examined by light microscopy for intergranular corrosion and photographed.

RESULTS

The polarization curves, obtained for the 430 stainless steel given the various heat-treatments, are shown in Figure 3. It is evident that the anodic currents are substantially higher for the samples heat treated in the critical temperature region.

Figures 4 and 5 show the current (i) vs time (t) plots at various applied potentials, for specimens aged at two different temperatures, along with the respective micrographs. From the i vs t plots and micrographs, it is clear that the passivation potential for the sample aged at 590°C is 200 mV_{SCE} and as per Figure 2, the minimum Cr level will be approximately 7%.

SENSITIZATION AND GRAIN BOUNDARY CORROSION

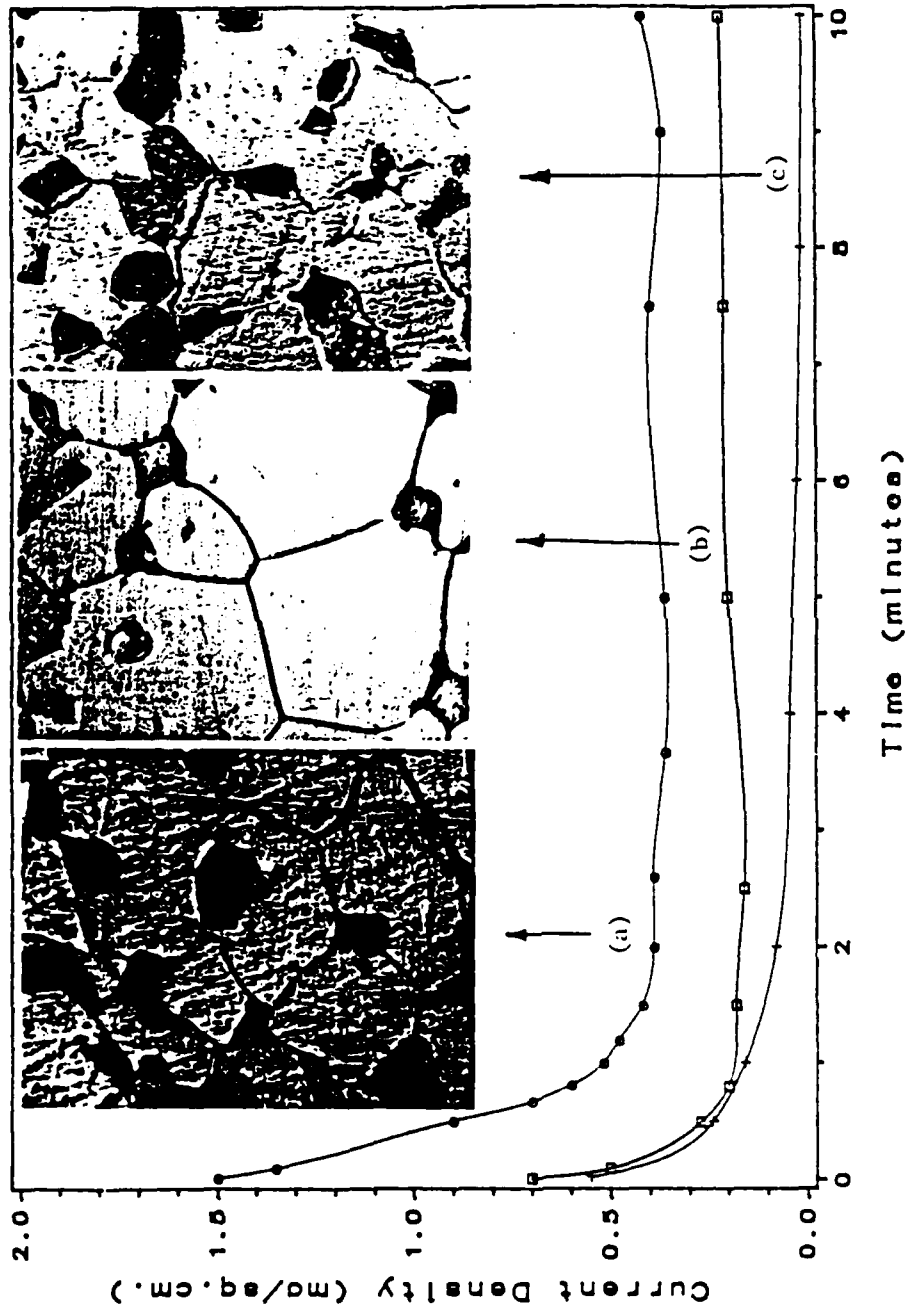


Figure 4. Current vs. time behavior at (a) -200, (b) 100, and (c) 200 mV_{SCE} and micrographs (at 400X) of the corroded surface for the specimen with heat treatment b in Figure 3.

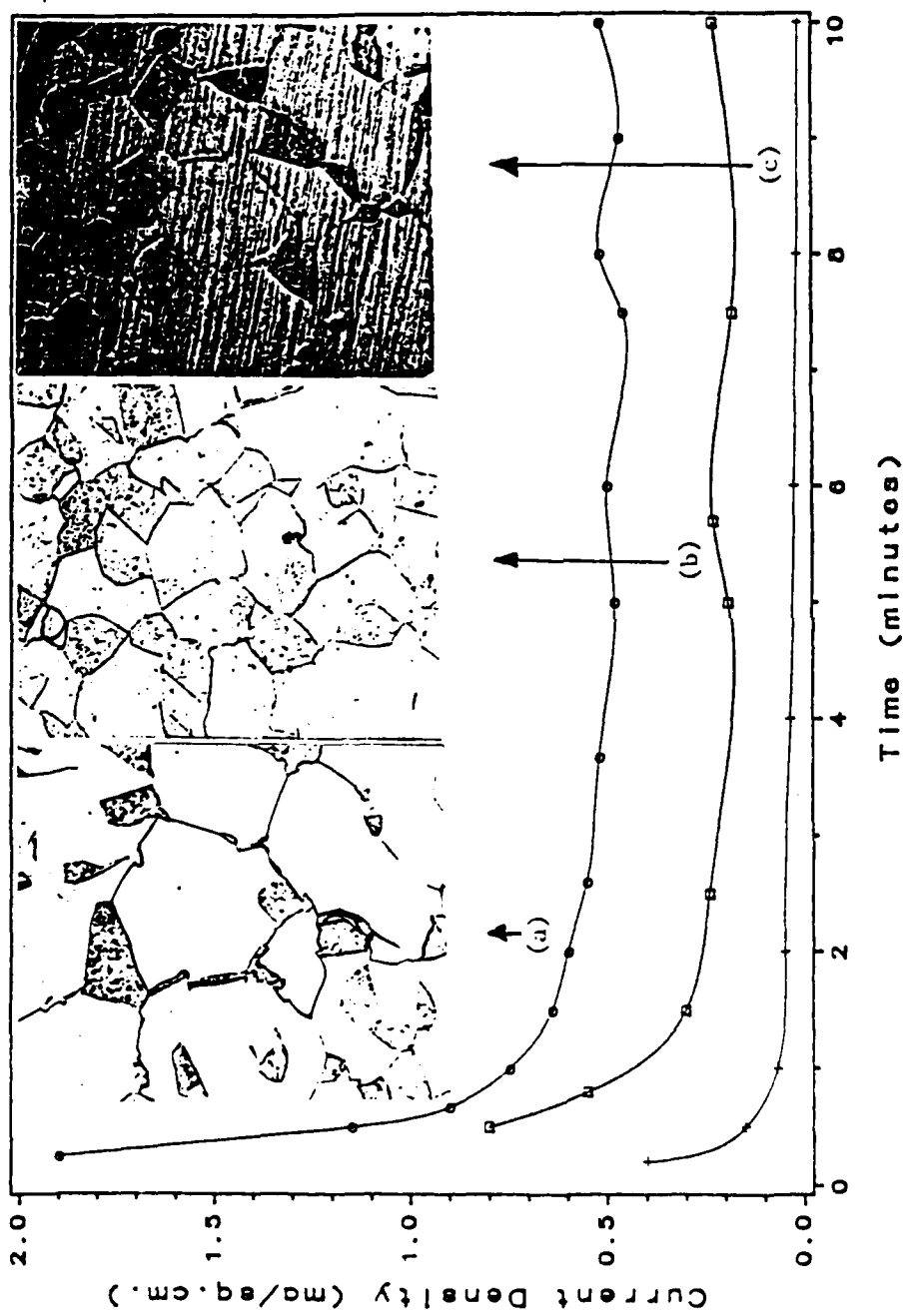


Figure 5. Current vs. time behavior at (a) 0, (b) 200, and (c) 300 mV_{SCF} and micrographs (at 400X) of the corroded surface for the specimen with heat treatment c in Figure 3.

SENSITIZATION AND GRAIN BOUNDARY CORROSION

For the sample aged at 475°C, the passivation potential is 300 mV_{SCE}, corresponding to a minimum Cr level of about 4%. Thus, the minimum Cr level in the sensitized alloy appears to be a function of the sensitization temperature, as predicted by the model.

DISCUSSION

From the foregoing results and analysis, it can be deduced that the sensitization temperature and bulk carbon concentration both play major roles in the sensitization process. Since the Cr diffusivity is quite high in ferritic stainless steels, it may be that the carbide growth that occurs during aging is partially controlled by the interface reaction, in which case the interfacial Cr concentration (Cr)_i will be higher than the equilibrium value. This is consistent with the result that the experimental values are higher than those predicted by the model, e.g., 1% vs 7% Cr for the 590°C aging. Results of Frankenthal and Pickering [4] indicated that the chromium concentration in the depleted zone can be much below 5% Cr, approaching 0% Cr. These differences in the measured Cr concentration could be due to an inherent inaccuracy in determining the exact passivation potential. Besides, it is a well known fact that carbide precipitation cannot be totally suppressed in bcc stainless steel even by quenching from 1200°C. Thus the nucleation and initial growth of these carbides occurs before aging. One of the factors that can effect the slowing of the interface reaction is a limiting carbon supply; thus, the interface reaction kinetics and Cr diffusion to the boundary become comparable kinetic processes. It is likely, however, that the dominance of either of these kinetic processes will vary among the grain boundaries of a sample and, thus, so will the Cr level, because of a number of other factors, such as grain boundary structure, habit planes and grain size.

Effect of Grain Boundary Structure and Habit Planes. The effect of grain boundary structure on intergranular corrosion [8] has been studied with the help of an Electron Backscattering technique used in conjunction with an SEM [22,23]. Analysis of the back scattered pattern yields information about the crystallography of individual grains, and by utilizing Rotation Matrix calculations [24,25], the grain boundary misorientation angles can be computed. Ideal atomic configurations at the grain boundaries can then be determined by knowing the orientation of the boundary plane from the SEM image [8].

To illustrate the above, a sample of the sensitized and corroded ferritic stainless steel (Fe-19Cr-0.09C) has been analyzed with the EBS technique. Figures 6(a) and (b) show the SEM image and the plot of corrosion groove width vs grain boundary misorientation angle between the labeled grains. The data in Figure 6(b) are consistent with the idea of a threshold misorientation angle for a particular aging condition, below which sensitization does not occur.

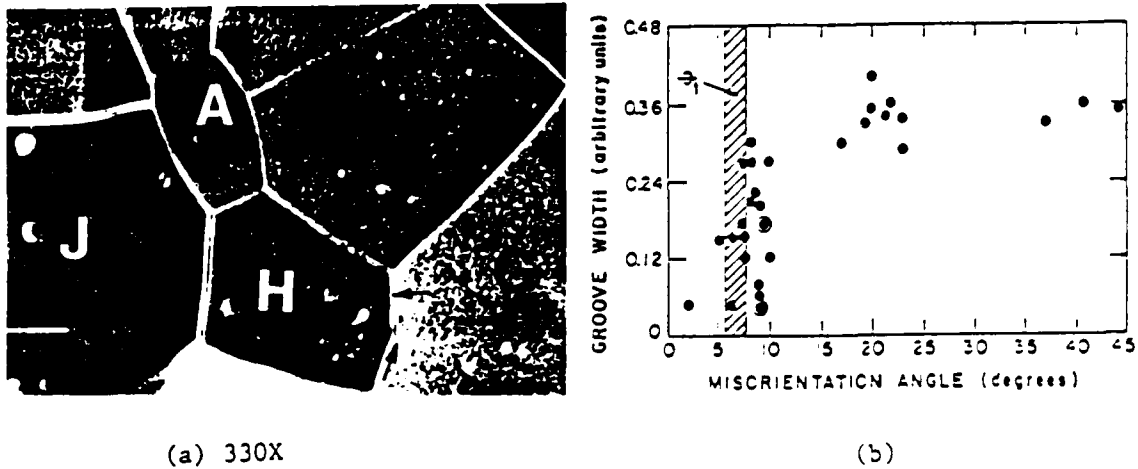


Figure 6. (a) SEM micrograph of a sensitized and anodically dissolved Fe-19Cr sample, illustrating a wide variation in the widths of the grain boundary grooves, (b) a plot of measured groove widths in Fe-19Cr sample, as a function of the misorientation angle. After Bennett and Pickering [8].

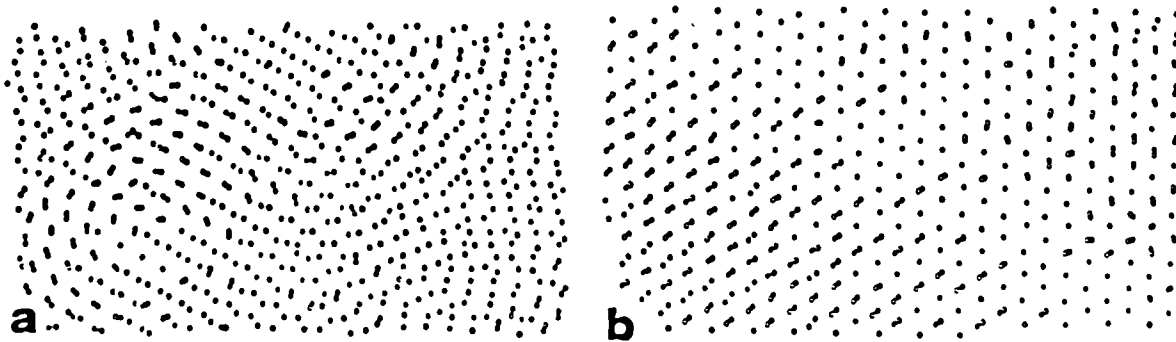


Figure 7. Computer generated ideal atomic arrangements of (a) upper segment (arrow normal to gb) of grain boundary G-H in Figure 6a, formed by superimposing the atomic arrangements of grains G and H, (b) lower segment of grain boundary G-H formed similar to (a) [8].

SENSITIZATION AND GRAIN BOUNDARY CORROSION

At a constant misorientation angle (9°) of the two segments of grain boundary between the grains G and H, the atomic configurations of these two segments, determined by the EBS technique [8,23], can be different; this is illustrated in Figure 7. It is evident that the lower boundary segment (arrow parallel to boundary in Figure 6a) has an atomic arrangement (Figure 7b) much more in coincidence than for the upper segment (Figure 7a). The observed groove widths reflect this i.e., 0.04 for the lower segment and 0.17 for the upper segment (circled points in Figure 6b). In other words, a grain boundary exhibiting a low coincidence of atomic sites sensitizes more readily and extensively.

The effect of habit planes on sensitization is much more difficult to establish. However, it is reasonable to expect that nucleation of $M_{23}C_6$ precipitate having a fcc structure [26] will favorably occur on $\{111\}$ planes along the $\langle 110 \rangle$ direction of the parent phase (bcc) since it can match with the $\{110\}$ planes along the $\langle 111 \rangle$ direction of the carbide (fcc). Thus, faceted and probably planar precipitates and puckered grain boundaries [27] can be the result. Therefore, those grain boundaries with boundary planes favorably oriented for carbide nucleation will be expected to have faceted precipitates towards the appropriate grain and the carbide will grow into this grain.

Effect of Grain Size. Since the carbide precipitation is occurring almost exclusively at the grain boundaries, it is expected for some conditions of mass transport and carbon content that the overall extent of sensitization would be proportional to the area of the grain boundary per unit volume of the alloy. Thus sensitization depends on grain size in that the amount of carbon available per unit area of boundary will be less for small than large grains. Assuming spherical grains of radius, r , the area of the grain boundaries per unit grain volume ($\frac{A}{V}$) can be plotted as a function of r ; a schematic plot is shown in Figure 8. Thus, considering a typical grain size distribution shown in Figure 9(a), the Cr depleted zone widths at the various grain boundaries will be different for certain aging times, as illustrated in Figure 9(b). Referring to Figure 6(a), it is apparent that the boundaries constituting grain A, which is the smallest grain, is the least corroded of all the boundaries. This observation reinforces the possible effect of grain size on sensitization. However, this effect is expected to taper off above a certain grain size regime for which the available carbon is adequate to fully sensitize all of the boundaries. This can be seen in Figure 8 where A/V approaches a constant value as r increases.

CONCLUSIONS

- (1) A thermodynamic model is presented that predicts the carbide-matrix interfacial Cr concentration at the grain boundaries of a ferritic stainless steel as functions of temperature and carbon content in the alloy.

- (2) An electrochemical technique was utilized to estimate the minimum level of Cr in the Cr depleted zone. The results of this measurement correlate with the model predictions on the temperature dependence of the carbide-matrix interfacial Cr concentration.
- (3) Sensitization occurs above a certain threshold misorientation angle. Boundaries with a large misfit or low coincidence of atomic sites sensitize much more.
- (4) In a certain grain size range a sample will exhibit differences in the extent of sensitization, owing to the differences in grain sizes: the finer the grain size, the less the sensitization.

ACKNOWLEDGEMENTS

The authors thank G. Was for helpful discussions of the model and computer program, L. Kaufman and D. Garvin for clarifications on thermodynamic data. Financial support of the Office of Naval Research under Contract No. N00014-84-k-0201 and supply of the alloy by Allegheny Ludlum Corp. are gratefully acknowledged.

REFERENCES

1. B. Strauss, H. Schottky and J. Hinnuber, *Z. anorg. allgem. Chem.*, **188**, 309 (1930).
2. E. C. Bain, R. H. Aborn and J. J. B. Rutherford, *Trans. Am. Soc. Steel Treating*, Vol. 21, p. 481 (1933).
3. C. Stawstrom and M. Hillert, *J. Iron & Steel Inst.*, Vol. 207, p. 77 (1969).
4. R. P. Frankenthal and H. W. Pickering, *J. Electrochem. Soc.*, Vol. 120, p. 23 (1973).
5. E. L. Hall and C. L. Briant, *Met. Trans.*, Vol. 15A, p. 793 (1984).
6. J. Lai, *Mat. Sci. & Eng.*, Vol. 58, p. 195 (1983).
7. J. Goldstein and E. Randich, *Met. Trans.*, Vol. 8A, p. 105 (1977).
8. B. W. Bennett and H. W. Pickering, "Effect of Grain Boundary Structure on sensitization and Corrosion of Stainless Steel", *Met. Trans.*, (in press).
9. G. S. Was and R. M. Kruger, *Acta Met.*, Vol. 33, No. 5, p. 841 (1985).
10. H. Wada, *Met. Trans.*, Vol. 17A, p. 1585 (1986).
11. F. Kohler, *Monatsh. Chemie*, Vol. 91, p. 738 (1960).
12. L. Kaufman, *CALPHAD*, Vol. 1, No. 1, p. 7-89 (1977).
13. R. Lundberg et al, *CALPHAD*, Vol. 1, No. 2, p. 159-199 (1977).
14. L. Kaufman and H. Nesor, *CALPHAD*, Vol. 2, No. 4, p. 295-318 (1978).
15. A. P. Bond, *Trans. Met. Soc. AIME*, Vol. 245, p. 2127 (1969).
16. M. A. Streicher, *Corrosion*, Vol. 29, No. 9, p. 337 (1973).
17. S. D. Conte and Carl de Boor, *Elementary Numerical Analysis*, 3rd edn., McGraw Hill Book Co., NY (1980).

SENSITIZATION AND GRAIN BOUNDARY CORROSION

18. F. B. Hildebrand, Method of Applied Mathematics, 2nd edn., Prentice Hall, Englewood Cliffs, NJ (1965).
19. M. Hillert, CALPHAD, Vol. 4, No. 1, p. 1 (1980).
20. C. J. Novak, Handbook of Stainless Steels, eds., D. Peckner and I. M. Bernstein, McGraw Hill, NY (1978), p. 4.1-4.77.
21. M. A. Streicher, J. Electrochem. Soc., Vol. 106, p. 161 (1959).
22. J. A. Venables and C. J. Harland, Phil. Mag., Ser. A., Vol. 27, p. 1193 (1973).
23. B. W. Bennett and H. W. Pickering, Scripta Met., Vol. 18, p. 743 (1984).
24. H. Grimmer, Acta. Cryst., Vol. A30, p. 685 (1974).
25. H. Mykura, in Grain Boundary Structure and Kinetics, ed. ASM, Metals Park, Ohio (1979), p. 445.
26. U. E. Wolff, Trans. Met. Soc. AIME, Vol. 236, p. 19 (1966).
27. J. K. Lee and H. I. Aaronson, Acta Met., Vol. 23, p. 799 (1975).

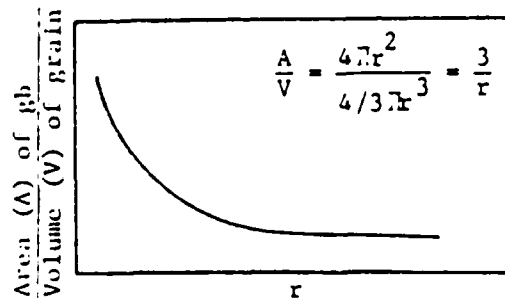


Figure 8. Schematic plot of area of grain boundaries per unit grain volume ($\frac{A}{V}$), as a function of grain radius, r .

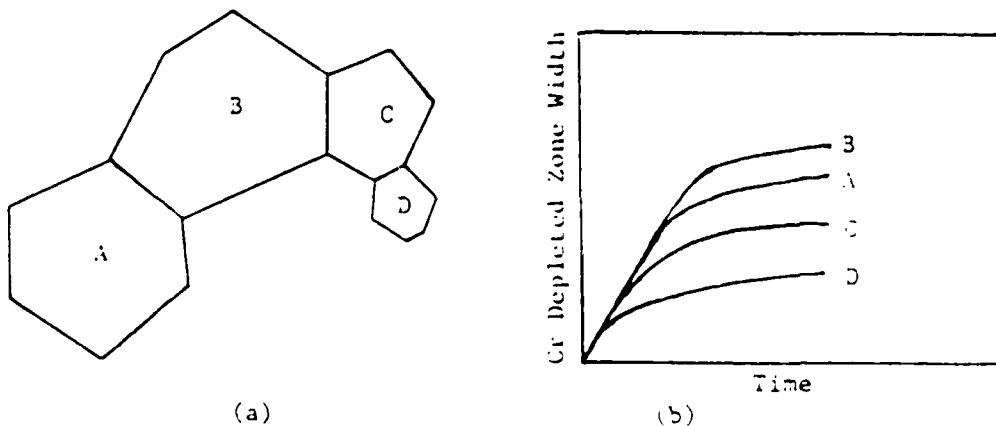


Figure 9. (a) Schematic grain size distribution in a sample, (b) schematic plot of Cr depleted zone width as a function of time, during isothermal aging for different grains in (a).

**THE LOCAL ELECTRODE POTENTIAL IN CAVITIES, CREVICES AND CRACKS AND ITS
ROLE IN CAUSING DEGRADATION OF STRUCTURAL MATERIALS**

Alberto Valdés and Howard W. Pickering

**The Pennsylvania State University
Department of Materials Science and Engineering
University Park, PA 16802, U.S.A.**

THE LOCAL ELECTRODE POTENTIAL IN CAVITIES, CREVICES AND CRACKS AND ITS ROLE IN CAUSING DEGRADATION OF STRUCTURAL MATERIALS

Alberto Valdés and Howard W. Pickering

The Pennsylvania State University
Department of Materials Science and Engineering
University Park, PA 16802, U.S.A.

ABSTRACT

In this work a traditionally disregarded point of view, the shift in the local electrode potential, is shown to be of great practical importance as well as a key factor from a theoretical perspective for understanding the localized corrosion problem. An active local condition can occur based solely upon electrode potential drops along cracks or crevices even in the absence of large gas and/or solid corrosion product accumulations.

INTRODUCTION

The magnitude of the potential drop that can be obtained in restricted environments such as pits, crevices and cracks has been an open controversy over the years. Both, supporters of their existence and opponents, are very strong on their convictions and none of them seem to yield ground to the other. What this ongoing controversy indicates is, that present day knowledge of the chemical and electrochemical conditions inside restricted environments is very limited. Thus, any contribution helping to clarify the whole picture is warmly welcomed.

A common feature of all growing pits, crevices and cracks is the restriction in the mass transport from the cavity to the bulk solution and vice versa. The most common of the naturally occurring phenomena conducive to this situation involves either the accumulation of solid corrosion products or the entrapment of gas bubbles within the walls of the cavity. The former has received a fair amount of

attention, see e.g. [1], but the second type concerning the effect of in-place bubbles on the electrode potential in a cavity has not been examined to its due extent, despite supporting experimental evidence showing definitively a possible new approach to pit initiation and growth. A paper reviewing these ideas has been published elsewhere [2,3], therefore no details will be presented here.

Existing reports in the literature show that large potential shifts (of the order of one volt) towards the active region have been found inside growing pits [4,5], and also that hydrogen gas evolved from these locations [5,6]. These results are not consistent with traditional theories of localized corrosion that invoke compositional differences in the electrolyte as the cause and ignore potential drops or with current models for pit growth that indicate a maximum expected potential drop within the electrolyte in the pit on the order of 100-300 mV [5,7,8]. It has also been shown that the large (1 Volt) potential drops within the pits were totally within the electrolyte phase, rather than within a film at the pit surface [5,9-11]. As a consequence of the latter, a contribution to the potential drop from an increased resistivity in the current path in the liquid has to be invoked.

Based on the fact that the evolution of hydrogen gas from the pits has been observed simultaneously with the large potential differences, the evidence is conclusive that the thermodynamic conditions for hydrogen gas evolution are met [5], which would be otherwise impossible if the local electrode potential in the crack was not much more reducing compared with the outer electrode surface potential, i.e. more negative than the hydrogen equilibrium potential. This shift of the electrode potential in the less oxidizing direction, corresponding to a decrease in the overpotential of the anodic metal dissolution reaction is bounded by the limiting potential (E_{lim}) of the system [12]. It follows that a portion of the pit in the potential region between E_{lim} and the active/passive potential will be undergoing active, rather than passive, dissolution [2,3].

The experiments described in this paper are designed to show the effects that the local electrode potential and the dissolution characteristics have on the events occurring in a crevice. Even though a theoretical treatment will not be presented, the importance of large potential changes in the occurrence of localized corrosion will be stressed.

The Local Electrode Potential in Cavities, Crevices and Cracks

EXPERIMENTAL

The material used throughout this work was Ferrovac-E iron; the specimens were cut from bars, degreased, heat treated at 800°C for two hours and furnace cooled. The experiments were carried out at pH 4.6 in a buffer solution of 0.5 M acetic acid and 0.5 M sodium acetate, some experiments were also carried-out with the addition of 0.005 M sodium chromate to the acetic buffer. All the solutions were prepared with reagent grade chemicals and double distilled water.

The experimental set-up used to make the measurements, shown in Figure 1, was a classical three electrode system. Observation of the events inside the crevice, and photographic recording of them, were possible with a stereo microscope viewing the crevice through the plexiglas plate. Luggin capillaries were used to monitor the control (applied) potential on the outside (top) surface and the local electrode potential at different positions inside the crevice. All the experiments were carried out under potentiostatic control in air saturated solutions.

A specimen, after polishing to a mirror-like surface, was placed in the Teflon™ holder and the plexiglas plate was attached to one of its surfaces to form an artificial crevice between the plexiglas and the metal wall; the crevice then consisted of one metallic side, four inert (plexiglas) walls and one opening (5mm x 0.5 mm) to the bulk of the solution; its depth was 10 mm.

The experimental procedure was as follows: the sample was first placed in the empty cell and all the necessary arrangements were made, with the sample under cathodic protection (generally -1 V) the electrolyte was added, the cathodic polarization was maintained until a constant current was reached in order to assure the removal of any air-formed film prior to the application of the anodic polarization. Once these conditions were obtained, the test was started. All records were time related to the moment at which the anodic polarization was first applied.

RESULTS AND DISCUSSION

A decrease in potential was found with an increase in the depth into the cavity, in the acetic buffer, in agreement with expected behaviour [9,13]. At the opening of the crevice the measured potential was close to the applied potential (+600 mV vs. SCE); towards the bottom the local potential reached an almost constant value of -570/-580 mV. For both gas-free and gas-occupied crevices, a large shift in potential occurred; when the shape of the bubble changed for any reason and did not fill completely the cross section, and even when the bubble was dislodged, the magnitude of the potential change in the crevice was in general the same; but, the potential change was less localized than for a gas filled cross section.

In fact, the presence of a non-conductive medium, the gas bubble in the present case, filling the cross section has the effect of a large resistance in the path of the current flowing through the cavity. The situation corresponds to the near isolation of the bottom of the crevice from the bulk of the solution, the only available path for current flow being the wedge shaped liquid regions between the bubble and the walls of the cavity. Similarly, wedge shaped liquid regions also exist between the bubble and the outside walls of the Luggin capillary probe when used to measure the local electrode potential underneath the bubble. These areas together add to a very small part of the entire cross section of the cavity and, as a result, only a very restrained region is available for current flow.

The significance of these potential variations can be better assessed if they are examined in the context of the current-potential response of a metal capable of having an active-passive behaviour. Figure 2 shows the classical shape of a polarization curve for such metals. It can be seen that due to the existing potential shift inside the crevice, from a point in the passive region (A) towards less noble values (B), the surface exhibits several characteristic features. For a given range of potentials, between A and the passivation potential, the metal is passive and no significant dissolution occurs. In the region of the passivation potential, a small further decrease in potential triggers a high dissolution current corresponding to the current maximum in the active region of the polarization curve. With further decrease in potential, corresponding to a greater distance into the crevice, the metal dissolution rate decreases in accordance with a decreasing

The Local Electrode Potential in Cavities, Crevices and Cracks

overpotential for the metal dissolution reaction. Simultaneously, the tendency for hydrogen evolution increases and at some distance into the cavity hydrogen evolution becomes thermodynamically possible. The passage of large metal dissolution currents in this limited region of the cavity wall below the passivation potential initiates a (new) crevice or trench at this site.

Thus, between the passive part of the metal in the cavity and the boundary of this new local crevicing action, an active/passive interface existed. It will be shown next that these features are present in a cavity that is supporting a local cell action.

Figure 3 shows a photographic sequence of the events in a crevice in the acetic buffer solution with the addition of chromate, without significant gas accumulation, after a potential in the passive region was applied to the outer (top) surface. In a short time a line representing an active/passive interface appeared (arrow), above which the crevice wall remained passive and below which passivity broke down. The metal below this transition was undergoing active dissolution, evidenced by the loss of the original metallic gloss which is still observable above the interface. This boundary initially moved upward as more of the surface became active. The rate of metal dissolution was high in the region identified by a bracket in the sixty minute photograph of Figure 3. Electrode potential measurements showed this (bracket) region of the crevice wall to correspond to the high current portion of the active loop of the polarization curve; due to the highest dissolution rate in this region, a new crevice appeared with time, as illustrated in Figure 4. After sixty minutes enough metal had been dissolved to make evident the start of a new local penetration (hereafter referred to as the crevice or active crevicing site) in this region of the cavity wall. After a longer time, this new crevice was well developed and appeared as a dark region due to the accumulation of corrosion products at this location (125 minute photograph).

The local cell (crevicing) in Figure 3 is shown schematically in Figure 4. The crevice advances with the highest rate of penetration occurring where the local electrode potential is in the peak region of the active loop (Figure 2). Figure 4 shows a long time consequence of its advancement. Surface perforations occurred as the crevice penetrated the outer (top) surface dissolving metal from underneath; once the penetration occurs, active dissolution ceases or slows considerably because the large IR drop that supports the active condition vanishes

the moment a new electrolyte path to the bulk solution exists. Other perforations of the surface will occur elsewhere. Similar "lace-like" surface perforations have been reported in the literature for other systems under completely different conditions [5,14]. Note that this explanation of these particular dissolution patterns is based on local potential variations rather than on local composition variations in the electrolyte.

The gas bubbles seen in Figure 3 are hydrogen since this is the only gas that can be generated at the local electrode potential existing in the crevice. Most of the initial bubbles were from the cathodic polarization applied at the beginning; but they were observed to grow rather than wane, after the potential was switched to the passive region. Their growth was by molecular diffusion of hydrogen generated in situ. The hydrogen bubbles grew continuously during anodic polarization of the outer (top) surface, which indicates that the growth was not due to the coalescence of residual hydrogen molecules from the cathodic treatment, but rather was due to the continuous generation of hydrogen molecules deep in the crevice where the potential was appropriate for this reaction. The hydrogen gas accumulation inside these restricted environments leads to an enhanced dissolution region at the boundary of the gas bubble [11]

CONCLUSIONS

The essential experimental results of this investigation are that large potential variations can exist in restricted environments giving rise to the establishment of local active cells. Large potential drops have for the first time been measured in the absence of accumulated gas in the cavity.

The finding of a large potential shift towards the active region calls for a whole new approach to the localized corrosion problem. This new approach must consider not only the traditional ideas of acidification and aggressive ion concentration build-up, but, also has to give the appropriate importance to local potential variations.

The role of potential variations in pits, crevices and cracks has been shown to be of great significance. In fact, the existence of the potential variations and the enhanced dissolution rate provides a viable explanation for some patterns of pit growth which have not previously been explained.

The Local Electrode Potential in Cavities, Crevices and Cracks

ACKNOWLEDGEMENTS

Financial support by the Office of Naval Research under Contract No. N00014-84-K-0201 is gratefully acknowledged. One of us (A.V.) wishes to express his gratitude to the Instituto Universitario de Tecnología - Región Capital and to Consejo Nacional de Investigaciones Científicas y Tecnológicas, both in Venezuela, for the support received.

REFERENCES

- [1] M. Pourbaix "The Electrochemical Basis for Localized Corrosion", pp 12-33 in International Conference on Localized Corrosion, R.W. Staehle et al, eds. National Association of Corrosion Engineers. 1974.
- [2] H. W. Pickering and A. Valdés. "A review of the effect of gas bubbles and cavity dimensions on the local electrode potential within pits, crevices and cracks", pp 33-48 in Symposium on Crack Chemistry and the Localized Environment, R.P. Gangloff, ed. American Society of Metals. 1983.
- [3] H.W. Pickering. "On the Roles of Corrosion Products in Local Cell Processes". Corrosion, 42, 125-40, (1985).
- [4] G. Herbsleb and H.J. Engell. "Untersuchungen über das Verhalten von aktivem und passiven Eisen in Schwefelsäure an über die Zerstörung der Passivschicht auf Eisen durch Chlorionen". Z. Elektrochem, 65, 881-7, (1961).
- [5] H.W. Pickering and R.P. Frankenthal. "On the Mechanism of Localized Corrosion of Iron and Stainless Steel". J. Electrochem. Soc., 119, 1297-310, (1972).
- [6] C.B. Bergeron and R.C. Benson. "Analysis of the gases Evolved during the Pitting Corrosion of Aluminum in various Electrolytes". J. Electrochem. Soc., 127, 2528-30, (1980).
- [7] D.A. Vermilyea and C.S. Tedmon, Jr. "A simple crevice corrosion theory". J. Electrochem. Soc., 117, 437-40, (1970).
- [8] T. R. Beck and E.A. Greens II. "An Electrochemical Mass Transport-Kinetic Model for Stress Corrosion Cracking of Titanium" J. Electrochem. Soc., 116, 177-84, (1969).

- [9] B.G. Ateya and H.W. Pickering. "On the Nature of Electrochemical Reactions at a Crack Tip during Hydrogen Charging of a Metal". *J. Electrochem. Soc.*, 122, 1018-26, (1975).
- [10] D. Harris and H.W. Pickering. "On Anodic Cracking During Cathodic Hydrogen Charging", pp 229-30 in Effect of Hydrogen on the Behaviour of Metals. A.W. Thompson and I.M. Bernstein, eds. American Institute of Mining, Metallurgical and Petroleum Engineers. 1975.
- [11] A. Valdés and H.W. Pickering, to be submitted to *J. Electrochem. Soc.*
- [12] H.W. Pickering. "The limiting IR Voltage within Electrolyte in Cavities during Localized Corrosion and Hydrogen charging of metals", pp 85-91 in H.H. Uhlig Symposium on Corrosion and Corrosion Protection, R.P. Fränkenthal and F. Mansfeld, eds. The Electrochemical Society, 1981.
- [13] B.G. Ateya and H.W. Pickering. "Electrochemical Processes within Cavities and Their Relation to Pitting and Cracking", pp 206-22 in Hydrogen in Metals, I.M. Bernstein and A.W. Thompson, eds. American Society of Metals. 1974.
- [14] J. Postlethwaite, B. Huber and D. Makepeace. "Hydrodynamic effects during electrochemical and exposure pitting test with passive metals". Paper No. 273. CORROSION 86. National Association of Corrosion Engineers. 1986.

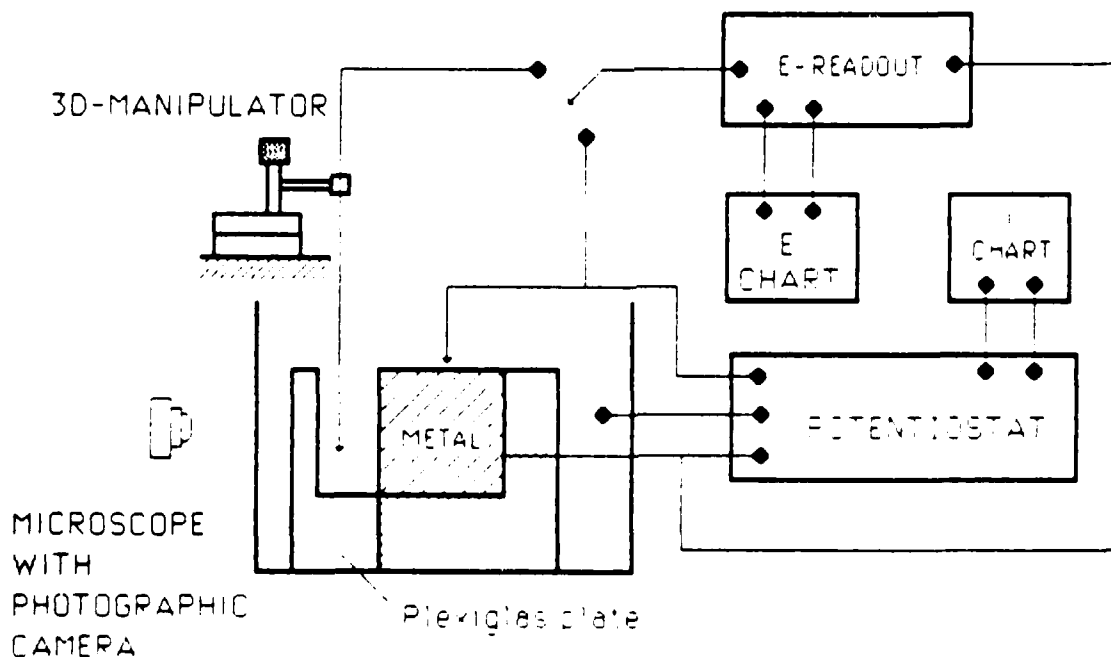


Figure 1. Schematic of the experimental set-up.

The Local Electrode Potential in Cavities, Crevices and Cracks

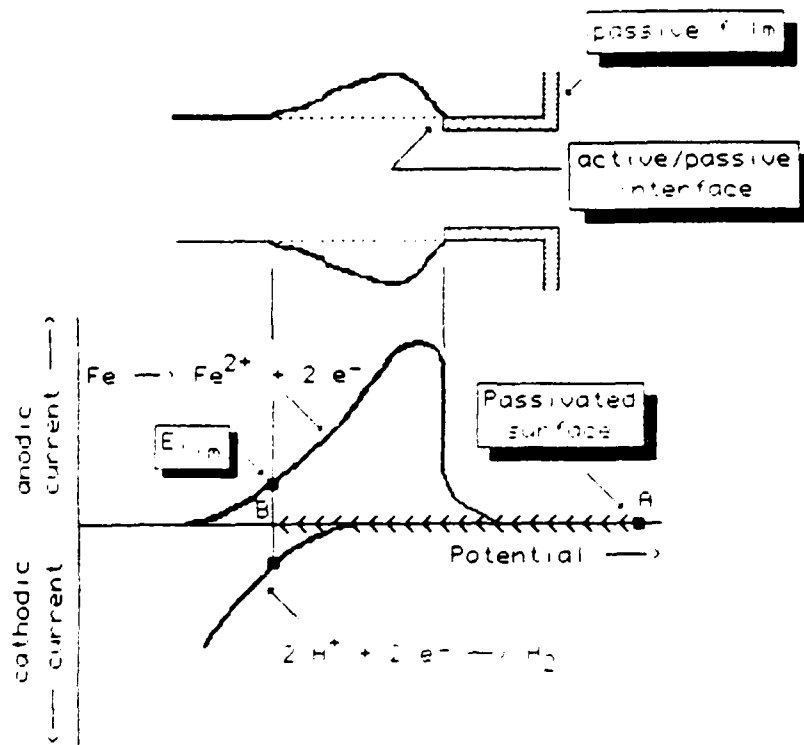


Figure 2 Schematic showing that for polarization of the surface at A the electrode potential in the crevice reaches B



Figure 4 (a) Advance of the new crevice; the shadowed region shows the dissolving surface (b) for long times the new crevice reaches the outer surface penetrating from underneath



5 minute



60 minute



125 minute

Figure 3. Views through the plexiglas of the iron wall in the crevice during anodic polarization of the differentiated iron surface at +600 mV vs SCE in 0.5 M acetic acid/0.5 M sodium acetate with 0.005 M sodium chromate. Below the line shown by the pointer passivity breaks down. Iron dissolution is rapid in the region shown by the bracket. Mag. 7X.

BASIC DISTRIBUTION LIST

Technical and Summary Reports

1985

<u>Organization</u>	<u>Code</u>	<u>Organization</u>	<u>Copies</u>
Defense Documentation Center Cameron Station Alexandria, VA 22314	12	Naval Air Propulsion Test Center Trenton, NJ 08628 ATTN: Library	1
Office of Naval Research Department of the Navy 800 N. Quincy Street Arlington, VA 22217 Attn: Codes 431	3	Naval Electronics Laboratory San Diego, CA 92152 ATTN: Electron Materials Sciences Division	1
Naval Research Laboratory Washington, DC 20375 ATTN: Codes 6000 6300 2627	1 1 1	Naval Missile Center Materials Consultant Code 3312-1 Point Mugu, CA 92041	1
Naval Air Development Center Code 606 Warminster, PA 18974 ATTN: Dr. J. DELuccia	1	Naval Construction Battallion Civil Engineering Laboratory Port Hueneme, CA 93043 ATTN: Materials division	1
Commanding Officer Naval Surface Weapons Center White Oak Laboratory Silver Spring, MD 20910 ATTN: Library	1	Commander David W. Taylor Naval Ship Research and Development Center Bethesda, MD 20084	1
Naval Oceans Systems Center San Diego, CA 92132 ATTN: Library	1	Naval Underwater System Center Newport, RI 02840 ATTN: Library	1
Naval Postgraduate School Monterey, CA 93940 ATTN: Mechanical Engineering Department	1	Naval Weapons Center China Lake, CA 93555 ATTN: Library	1
Naval Air Systems Command Washington, DC 20360 ATTN: Code 310A Code 5304B	1 1	NASA Lewis Research Center 21000 Brookpark Road Cleveland, OH 44135 ATTN: Library	1
Naval Sea System Command Washington, DC 20362 ATTN: Code 05R	1	National Bureau of Standards Washington, DC 20234 ATTN: Metals Science and Stands Division Ceramics Glass and Solid State Science Division Fracture and Deformation Div.	1 1 1

Supplemental Distribution List

Jan 1985

Prof. I.M. Bernstein
Dept. of Metallurgy and Materials Science
Carnegie-Mellon University
Pittsburgh, PA 15213

Prof. H.K. Birnbaum
Dept. of Metallurgy & Mining Eng.
University of Illinois
Urbana, Ill 61801

Dr. D.H. Boone
Department of Mechanical Eng.
Naval Postgraduate School
Monterey, Ca 93943

Dr. C.R. Crowe
Code 6372
Naval Research Laboratory
Washington, D.C. 20375

Prof. D.J. Duquette
Dept. of Metallurgical Eng.
Rensselaer Polytechnic Inst.
Troy, NY 12181

Prof. J. P. Hirth
Dept. of Metallurgical Eng
The Ohio State University
Columbus, OH 43210

Dr. R.G. Kasper
Code 4493
Naval Underwater Systems Center
New London, CT 06320

Prof. H. Leidheiser, Jr.
Center for coatings and Surface Research
Sinclair Laboratory, Bld. No. 7
Lehigh University
Bethlehem, PA 18015

Dr. F. Mansfeld
Rockwell International - Science Center
1049 Camino Dos Rios
P.O. Box 1085
Thousand Oaks CA 91320

Profs. G.H. Meier and F.S. Pettit
Dept. of Metallurgical and
Materials Eng.
University of Pittsburgh
Pittsburgh, PA 15261

Dr. J.R. Pickens
Martin Marietta Laboratories
1450 South Rolling Rd.
Baltimore, MD 21227-3898

Prof. H.W. Pickering
Dept. of Materials Science and
Eng.
The Pennsylvania State
University
University Park, PA 16802

Prof. R. Summit
Dept. of Metallurgy Mechanics
and Materials Science
Michigan State University
East Lansing, MI 48824

Prof. R.P. Wei
Dept. of Mechanical Engineering
and Mechanics
Lehigh University
Bethlehem, PA 18015

Prof. A.J. Ardell
Dept. of Materials Science and Eng.
School of Engineering & Applied
Science
University of California at
Los Angeles
Los Angeles, CA 90024

Prof. B.E. Wilde
Fontana Corrosion Center
Dept. of Metallurgical Eng.
The Ohio State University
116 west 19th Ave.
Columbus, OH 43210

Dr. C. R. Clayton
Department of Materials Science
& Engineering
State University of New York
Stony Brook
Long Island, New York 11794

Naval Facilities Engineering Command Alexandria, VA 22331 ATTN: Code 03	1	Defense Metals and Ceramics Information Center Battelle Memorial Institute 505 King Avenue Columbus, Oh 43201	1
Scientific Advisor Commandant of the Marine Corps Washington, DC 20380 ATTN: Code AX	1	Metals and Ceramics Division Oak Ridge National Laboratory P.O. Box X Oak Ridge, TN 37380	1
Army Research Office P. O. Box 12211 Triangle Park, NC 27709 ATTN: Metallurgy & Ceramics Program	1	Los Alamos Scientific Laboratory P.O. Box 1663 Los Alamos, NM 87544 ATTN: Report Librarian	1
Army Materials and Mechanics Research Center Watertown, MA 02172 ATTN: Research Programs Office	1	Argonne National Laboratory Metallurgy Division P.O. Box 229 Lemont, IL 60439	1
Air Force Office of Scientific Research/NE Building 410 Bolling Air force Base Washington, DC 20332 ATTN: Electronics & Materials Science Directorate	1	Brookhaven National Laboratory Technical Information Division Upton, Long Island New York 11973 ATTN: REsearch Library	1
NASA Headquarters Washington, DC 20546 ATTN: Code RRM	1	Library Building 50 Room 134 Lawrence Radiation Laboratory Berkeley, CA	1
Mr. Michael T. McCracken Office of Naval Research Resident Representative National Academy of Sciences, Joseph Henry Bldg., Room 623, 2100 Pennsylvania Avenue, N.W. Washington, D.C. 20037	1		

END

4-87

DTIC